The Effect of Stokes Drift and Transient Rip Currents on the Inner Shelf. Part II: With Stratification

NIRNIMESH KUMAR

University of Washington, Seattle, Washington

FALK FEDDERSEN

Scripps Institution of Oceanography, La Jolla, California

(Manuscript received 30 March 2016, in final form 17 November 2016)

ABSTRACT

This is Part II of a two-part study focused on Stokes drift and transient rip current (TRC) effects on the unstratified (Part I) and stratified (this paper) inner shelf. Part I focuses on funwaveC–Coupled Ocean–Atmosphere–Wave–Sediment Transport (COAWST) coupling and TRC effects on mixing and exchange on an unstratified inner shelf. Here, two simulations (R3 and R4) are performed on a stratified inner shelf and surfzone with typical bathymetry, stratification, and wave conditions. R3 is a COAWST-only simulation (no TRCs), while R4 has funwaveC–COAWST coupling (with TRCs). In R4, TRCs lead to patchy, near-surface cooling, vertical isotherm displacement, and increased water column mixing. For both R3 and R4, the mean Lagrangian circulation has two nearly isolated surfzones and inner-shelf overturning circulation cells, with a stronger, R4, inner-shelf circulation cell. The R4, inner-shelf, vertical velocity variability is 2–3 times stronger than a simulation with TRCs and no stratification. Relative to R3, R4 eddy diffusivity is strongly elevated out to three surfzone widths offshore due to TRCs and TRC-induced density overturns. The R4 inner-shelf stratification is reduced nearshore, and mean isotherms slope more strongly than R3 because of the TRC-enhanced irreversible mixing. At six surfzone widths offshore, both R3 and R4 are in geostrophic balance, explaining the stratified (summertime) observed deviation from Stokes–Coriolis balance. In this region, baroclinic pressure gradients induced by sloping isotherms induce an alongshore geostrophic jet offshore, strongest in R4. In R4, TRCs result in an enhanced (2–10 times) cross-shore exchange velocity across the entire inner shelf, relative to R3. Accurate, stratified, inner-shelf simulations of pollution, larval, or sediment transport must include transient rip currents.

1. Introduction

This is Part II of a two-part study that focuses on exploring Stokes drift–driven and transient rip current effects on an unstratified (Kumar and Feddersen 2016, hereinafter Part I) and a stratified (Part II, this manuscript) inner shelf. Background and motivation is provided in Part I and is revisited here as relevant to the stratified inner shelf. The nearshore region consists of the surfzone [from the shoreline to the seaward extent of depth-limited breaking (L_{SZ})] to the inner shelf (from 5 to $\approx$15 m). Surfzone and inner-shelf cross-shelf exchange processes, important for tracer evolution (e.g., larvae, pollutants), are three-dimensional, complex, and forced by a variety of mechanisms. However, the relative role of surface gravity wave–driven processes, such as Stokes drift and transient rip currents, in driving cross-shore exchange on a stratified inner shelf is not understood.

On an alongshore uniform bathymetry, cross-shelf exchange from the surfzone across the inner shelf is often due to a nonzero, mean, cross-shore Lagrangian circulation in the vertical z and cross-shore x plane, where the mean, cross-shore Lagrangian velocity $\overline{u}_L(z) = \overline{u}_e(z) + \overline{u}_{st}(z)$ is the sum of the mean Eulerian velocity $\overline{u}_e$ and the onshore, wave-driven Stokes drift $\overline{u}_{st}$ (e.g., Lentz and Fewings 2012). In particular, for inner-shelf weak vertical mixing (e.g., weak winds) and weak

Denotes content that is immediately available upon publication as open access.

Corresponding author e-mail: N. Kumar, nirni@uw.edu

DOI: 10.1175/JPO-D-16-0077.1

lateral variations, a Stokes–Coriolis balance (e.g., Xu and Bowen 1994; Lentz et al. 2008) develops:

$$f\overline{u}_e(z) = -f\overline{u}_{\mathrm{st}}(z), \tag{1}$$

where f is the Coriolis parameter, resulting in zero-mean Lagrangian flow $\overline{u}_L = 0$ and no cross-shelf exchange. For subtidally (>33-h time scale) averaged, Eulerian, cross-shelf velocities and unstratified conditions, a Stokes–Coriolis balance (1) was observed in $h = 12$-m depth for weak winds (Lentz et al. 2008). However, for summer (stratified) conditions, near the bed $\overline{u}_L$ was onshore, and in the upper–midpart of the water column $\overline{u}_L$ was offshore, inconsistent with a Stokes–Coriolis balance (Lentz et al. 2008). This result was unexpected, as weak vertical mixing due to stratification should allow Stokes–Coriolis balance to dominate. However, spatial variation in stratification, wave forcing, or other processes may have been important (Lentz et al. 2008).

On an alongshore, uniform bathymetry, exchange from the surfzone across the inner shelf is also induced by horizontal eddies (vertical vorticity). Finite-crest-length wave breaking generates surfzone eddies (Peregrine 1998; Johnson and Pattiaratchi 2006; Spydell and Feddersen 2009; Clark et al. 2012; Feddersen 2014) that coalesce, inducing episodic, 10–50-m, alongshore, length-scale transient rip currents (TRCs) that dominate (over nonzero $\overline{u}_L$) observed and modeled surfzone to inner-shelf exchange (Hally-Rosendahl et al. 2014, 2015; Hally-Rosendahl and Feddersen 2016). Even in the inner-shelf TRC-generated, eddy-induced exchange is larger than an estimated Stokes drift–driven exchange for two to five surfzone widths L_{SZ}, as indicated through a depth-integrated, wave-resolving model study (Suanda and Feddersen 2015).

Inner-shelf stratification can be strong even within 80 m of the surfzone inhibiting vertical tracer mixing (Hally-Rosendahl et al. 2014). A stratified inner shelf enhances cross-shelf exchange due to cross-shelf winds in both observations (Fewings et al. 2008) and models (Tilburg 2003; Horwitz and Lentz 2014), relative to an unstratified inner shelf. On a stratified inner shelf, TRCs also have associated temperature signals (Marmorino et al. 2013; Hally-Rosendahl et al. 2014), suggesting their role in inner-shelf temperature evolution. However, for a stratified inner shelf, the effects of Stokes drift and TRCs on mean Lagrangian circulation, inner-shelf eddies, temperature evolution, mixing, momentum dynamics, and cross-shelf exchange is poorly understood.

Three-dimensional (3D) transient rip currents and Stokes drift–driven flow on a stratified inner shelf have never been modeled before. In Part I, the wave-resolving Boussinesq model funwaveC is coupled to a wave-averaged, depth- and stratification-resolving model, Coupled Ocean–Atmosphere–Wave–Sediment Transport (COAWST), to allow both Stokes drift effects and 3D TRCs on an unstratified inner shelf. Relative to simulations without TRCs, TRCs induced significant changes in the mean overturning Lagrangian circulation, velocity variability, mean eddy viscosity, momentum balances, and exchange velocity out to $5L_{\mathrm{SZ}}$ offshore.

Here in Part II, the work in Part I is extended to a stratified inner shelf with a single-case example having typical bathymetry, stratification, and waves but no wind. Two simulations are analyzed and contrasted, one without (R3) and one with (R4) TRC effects, analogous to R1 and R2 in the unstratified Part I. Here, the focus is on the effect of Stokes drift and TRCs on the mean overturning Lagrangian circulation, velocity variability, temperature evolution, mixing, momentum balances, and a cross-shelf exchange velocity on the stratified inner shelf.

A detailed model description and validation is provided in Part I and briefly described for a stratified inner shelf (section 2). The surfzone and inner-shelf temperature evolution over 48 h both without (R3) and with (R4) TRCs is described in section 3. The effect of TRCs on the inner-shelf mean Lagrangian overturning streamfunction, eddy variability, mean vertical eddy viscosity, and mean temperature are examined in section 4. The discussion (section 5) examines mean cross-shore momentum balances, irreversible mixing, and cross-shore exchange velocity both with and without TRCs. Last, the development of an inner-shelf, alongshore, geostrophic jet is explained. The results are summarized in section 6.

2. Methods

a. funwaveC model description and configuration

The open-source, wave-resolving Boussinesq model funwaveC (e.g., Feddersen 2007; Spydell and Feddersen 2009; Feddersen et al. 2011; Clark et al. 2012; Guza and Feddersen 2012; Feddersen 2014; Suanda and Feddersen 2015; Hally-Rosendahl and Feddersen 2016) is described in detail elsewhere (Feddersen et al. 2011). Model configuration is discussed in Part I, with a quick summary provided here. The funwaveC simulation generates a transient rip current due to normally incident random directional waves on an alongshore, uniform planar beach with slope 0.025 to depth $h = 7$ m and constant h farther offshore. The total cross-shore x and alongshore y domain lengths are 500 and 1000 m, respectively, with cross- and alongshore grid sizes of $\Delta x = 1.25$ m and $\Delta y = 1$ m. The alongshore boundary conditions are periodic. Random directionally spread waves with significant wave height $H_s = 1$ m, peak period $T_p = 10$ s, bulk (mean) wave angle $\overline{\theta} = 0°$, and directional spread $\sigma_\theta = 10°$ allow vorticity generation due to finite-crested wave breaking (Peregrine 1998). Model variables are output at 1 Hz. The funwaveC-simulated curl of the breaking wave that generates surfzone vertical vorticity (eddies) on a variety of length scales (Feddersen 2014) is expressed using a scalar forcing streamfunction ψ_F:

$$\nabla \times \mathbf{F}_{\mathrm{br}} = \nabla^2 \psi_F. \tag{2}$$

The streamfunction ψ_F is solved for at 1 Hz (e.g., Spydell and Feddersen 2009) and stored for input to COAWST (section 2b).

b. COAWST model description and configuration

The COAWST model (Warner et al. 2010) couples the circulation model ROMS and the wave model Simulating Waves Nearshore (SWAN) and has been validated in a range of surfzone, estuary, and inner-shelf scenarios in the subtidal and tidal band (e.g., Kumar et al. 2012; Olabarrieta et al. 2011; Kumar et al. 2015b,a). However, wave-averaged COAWST cannot simulate transient rip currents through surfzone eddies generated by finite-crested wave breaking, motivating the coupling with funwaveC.

Detailed model setup is provided in Part I. The bathymetry $h(x)$ is alongshore uniform. The cross-shore profile (thick solid black line, Fig. 1) is planar with slope 0.025 to $h = 7$-m depth, matching the funwaveC bathymetry. Farther offshore the bathymetry is concave and the slope reduces to the typical, Southern California, inner-shelf bathymetry profiles (Kumar et al. 2015b). The COAWST model domain is 1000 m in the alongshore and 800 m in the cross shore with grid resolution of $\Delta x = 1.25$ m and $\Delta y = 2$ m. The alongshore boundary conditions are periodic. Here, ROMS has 10 bathymetry-following vertical levels and the Coriolis parameter $f = 8.09 \times 10^{-5}\,\mathrm{s}^{-1}$ is typical for Southern California. In contrast to Part I, the simulations here are run for 48 h (2 days) with a ROMS baroclinic time step of 0.25 s and barotropic time step of 0.0125 s.

At the SWAN offshore boundary, the wave field ($H_s = 0.95$ m, peak period $T_p = 10$ s, mean wave direction $\overline{\theta} = 0°$, and a directional spread $\sigma_\theta = 10°$) is prescribed to match funwaveC at $x > -280$ m. SWAN cross shore evolves the wave field with standard parameters. SWAN- and funwaveC-modeled H_s compare well (Part I), indicating that the two models evolve waves consistently. SWAN-derived, vertically varying Stokes drift $\overline{u}_{\mathrm{st}}(z)$ drives circulation in ROMS with one-way coupling (Part I). COAWST surfzone eddy generation is given by the funwaveC rotational wave forcing [i.e., $\nabla \times \psi_F(x, y, t)\mathbf{k}$, where $\mathbf{k}$ is the upward unit vector] as a depth-uniform body force at 1 Hz. As the funwaveC simulation is for 12 h, this body force is symmetric from 1 to 12 h and from 12 to 24 h, and similarly from 24 to 36 h and from 36 to 48 h.

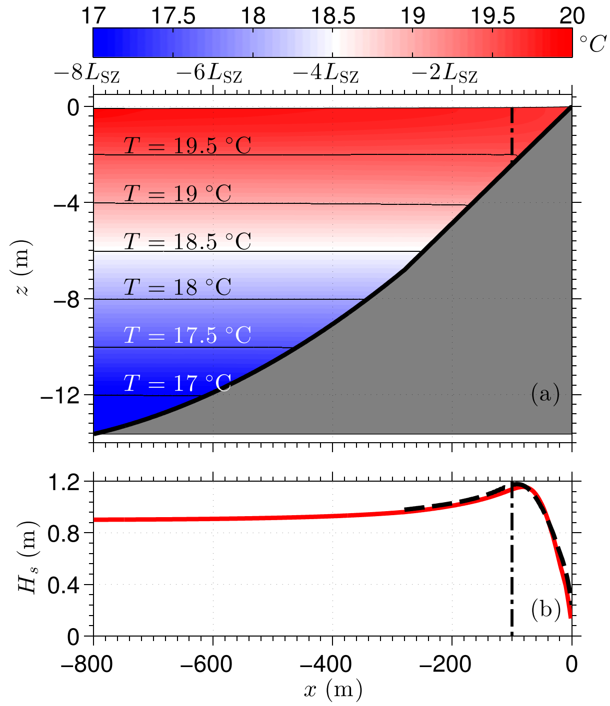

FIG. 1. (a) COAWST cross-shore bathymetry (thick solid black line) and temperature initial condition (colors and contours). The stratification of $\partial T/\partial z = 0.25°\mathrm{C\,m^{-1}}$ corresponds to $N^2 = 6 \times 10^{-4}\,\mathrm{s}^{-2}$, typical for the Southern California inner shelf. (b) Significant wave height H_s for SWAN (red) and funwaveC (black dashed). In (a) and (b), the vertical dashed–dotted line delimits the surfzone $x = -L_{\mathrm{SZ}}$ (where $L_{\mathrm{SZ}} = 100$ m).

The ROMS temperature initial condition is $T = 20°\mathrm{C}$ at $z = 0$ m, with constant stratification of $\partial T/\partial z = 0.25°\mathrm{C\,m^{-1}}$ everywhere (surfzone and inner shelf) such that at $z = -12$ m, $T = 17°\mathrm{C}$ (Fig. 1). This stratification corresponds to $N^2 = 6 \times 10^{-4}\,\mathrm{s}^{-2}$, which is typical for the Southern California Bight (Omand et al. 2012; Hally-Rosendahl et al. 2014; Kumar et al. 2015b). At the offshore boundary ($x = -800$ m), temperature is kept fixed to the initial condition. Solar heating and air–sea fluxes, which can also modify water column temperature, are not considered in this study.

c. COAWST stratified simulations R3 and R4: Without and with transient rip currents

In Part I, two unstratified COAWST simulations R1 and R2 were conducted without (R1) and with (R2) transient rip currents generated by the coupling to funwaveC. Similarly, here, two stratified COAWST simulations are performed, one without (R3) and one with (R4) transient rip currents generated by coupling to funwaveC. Both simulations have identical initial stratifications (Fig. 1).

3. Results: Effects of Stokes drift and transient rip currents on a stratified inner shelf—Temperature evolution

Here, the stratified inner-shelf temperature and vorticity evolution over 48 h is examined for the case without (R3) and with (R4) transient rip currents.

a. Inner-shelf temperature evolution without transient rip currents: R3

Here, R3 instantaneous temperature evolution is examined after 6 (0 h is model start time) and 48 h have elapsed (Fig. 2). After 6 h, the surfzone ($x > -L_{SZ}$) temperature is vertically well mixed (unstratified; Fig. 2a) from its stratified initial condition. Offshore of the surfzone at $x = -2L_{SZ}$ and $x = -3L_{SZ}$, the stratification is reduced 25% and 15%, respectively, of the initial $\partial T/\partial z = 0.25°\mathrm{C\,m^{-1}}$ (Fig. 2a). Farther offshore at $x < -4L_{SZ}$, stratification is close to the initial stratification. This slow temperature evolution is driven by the mean Lagrangian circulation (onshore Stokes drift and offshore undertow) coupled with strong surfzone vertical mixing. Thus, relatively warmer near-surface waters enter the surfzone and relatively colder well-mixed water leaves the surfzone. At 48 h stratification is reduced (Fig. 2b). At $x = -2L_{SZ}$ and $x = -3L_{SZ}$, $\partial T/\partial z$ is reduced 60% and 36%, respectively, relative to the original stratification. However, farther offshore at $x \le -4L_{SZ}$, the stratification remains close to the initial stratification (Fig. 2b$_2$). The processes driving this R3 (no TRCs) temperature evolution pattern are discussed later.

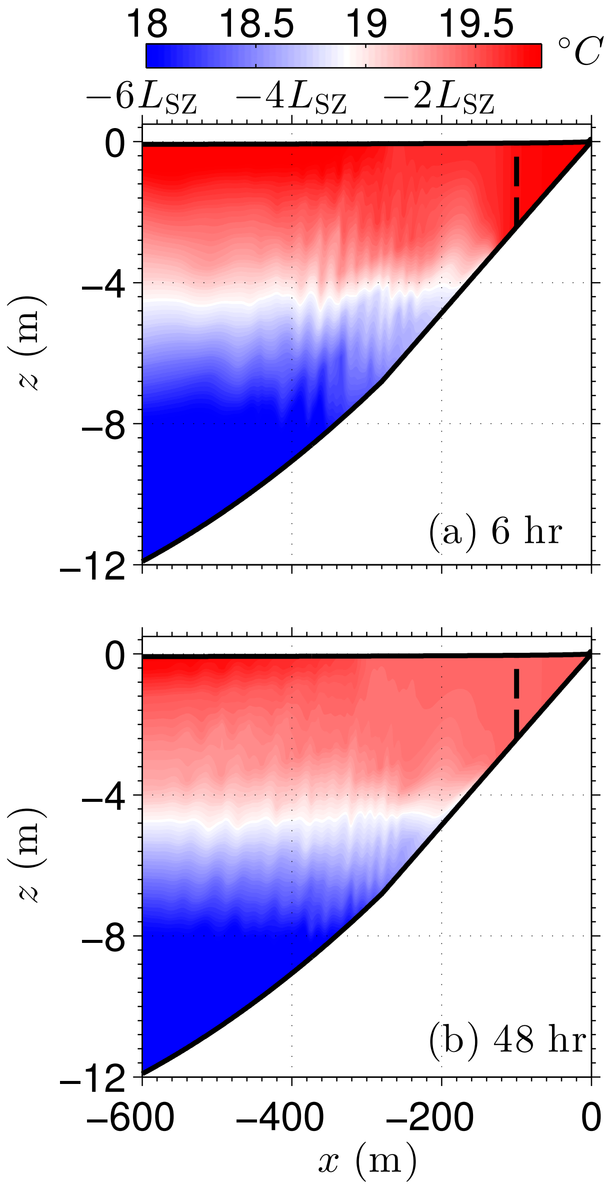

FIG. 2. R3 (no TRCs) simulated temperature T at (a) 6 and (b) 48 h. Dashed black line delimits the surfzone $x = -L_{SZ}$.

b. Inner-shelf temperature evolution with transient rip currents: R4

Here, R4 (with TRCs) modeled vorticity and temperature evolution is examined over 48 h and contrasted with R3 (Figs. 3–5). In Part I, TRC ejection onto the unstratified inner shelf (R2) strongly influenced the mean overturning Lagrangian circulation, vertical eddy viscosity, and cross-shelf exchange flow out to $x = -3L_{SZ}$. With stratification, the R4, modeled, near-surface ($z = -1$ m) vorticity is qualitatively similar to R2 (see Part I) both for the first 24 h of simulation (Figs. 3a1–a4) and 24–48 h of simulation (Figs. 4a1–a4). The R4 surfzone vorticity field is highly variable with a range of length scales similar to R2 and funwaveC (Part I; Feddersen 2014). R4 inner-shelf eddy variability extends offshore to $x = -3L_{SZ}$ with vorticity monopoles, dipoles, filaments, and streaks at $O(10^{-2})\,\mathrm{s^{-1}}$, much larger than the Coriolis parameter. At 6 h and onward the eddy field has equilibrated at $x > -4L_{SZ}$ (left columns, Figs. 3 and 4).

TRCs and the resulting inner-shelf eddy field strongly affect the R4 temperature evolution over 48 h (center and right columns, Figs. 3 and 4) through stirring and mixing. At 1 h, the R4, near-surface ($z = -1$ m), inner-shelf temperature $T(x, y)$ is mostly ≥19.6°C with a few cold patches (≤19.4°C) extending out to $x = -3L_{SZ}$ with

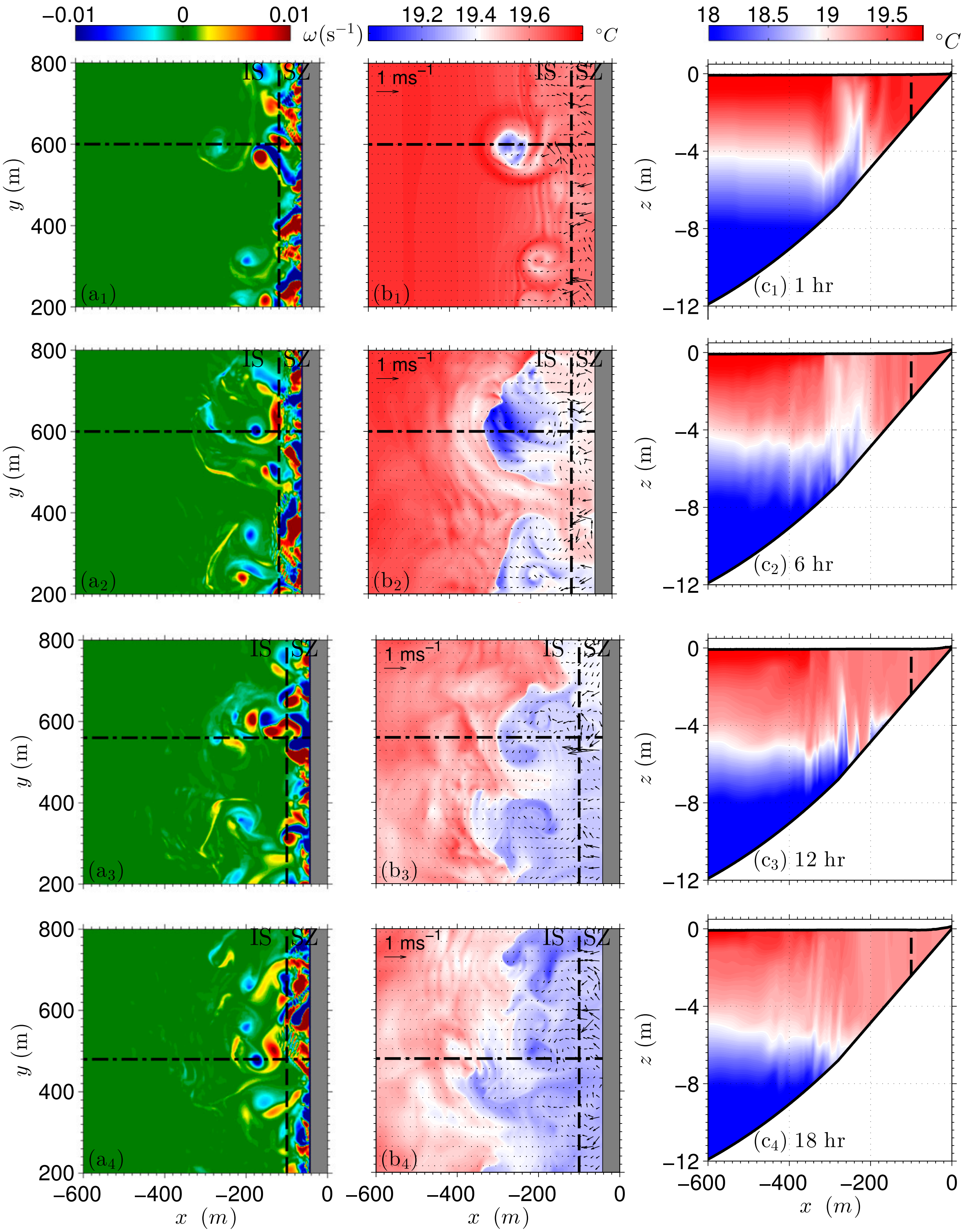

FIG. 3. R4 (with TRCs) simulated (left) vertical vorticity and (center) temperature at $z = 1$ m; and (right) temperature at the dashed–dotted line at times (a_1),(b_1),(c_1) 1, (a_2),(b_2),(c_2) 6, (a_3),(b_3),(c_3) 12, and (a_4),(b_4),(c_4) 18 h. Dashed black line delimits the surfzone $x = -L_{SZ}$.

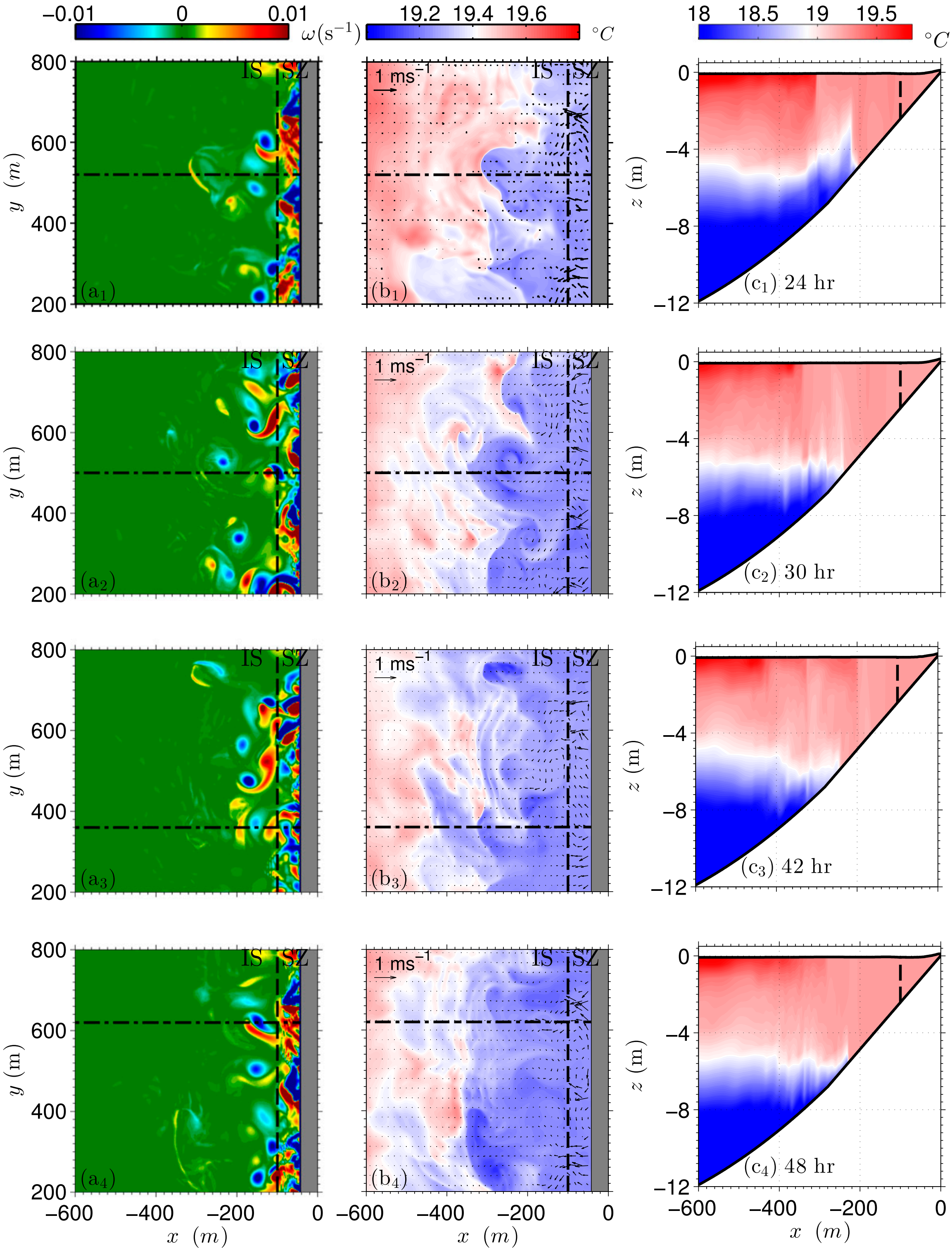

FIG. 4. As in Fig 3, but at times $(a_1),(b_1),(c_1)$ 24, $(a_2),(b_2),(c_2)$ 30, $(a_3),(b_3),(c_3)$ 42, and $(a_4),(b_4),(c_4)$ 48 h.

scales of 100 m (Fig. 3b1), corresponding to TRC ejection locations (Fig. 3a1). At $y = 600$ m (dashed–dotted line in Fig. 3b1), the surfzone is vertically well mixed with $T(x, z) = 19.6°C$ (Fig. 3c1), similar to R3. Farther offshore at $x = -2.5L_{SZ}$, the isotherms are elevated up to 3 m at the cold patch location, and just offshore at $x = -3.5L_{SZ}$ the isotherms are depressed up to 2 m (Fig. 3c1). These R4 temperature features starkly contrast to those of R3 (Fig. 2).

At 6 h, R4 near-surface temperature is cooler (down to $T = 19.2°C$) out to $x = -4L_{SZ}$ with larger 200-m length scales (Fig. 3a2) compared to at 1 h. At 6 h, the R4 (with TRCs) near-surface T is much cooler and more variable. At $y = 600$ m, the well-mixed surfzone has cooled further with $T(x, z) = 19.3°C$ (Fig. 3c2), much cooler than R3. Farther offshore at $x = -3L_{SZ}$, the $T = 19°C$ isotherm forms an eddy temperature front (Fig. 3c2), while near $x = -6L_{SZ}$, R4 temperature is similar to the initial condition and R3. Transient rip currents result in strong vertical mixing, reducing the stratification at $x \geq -3L_{SZ}$ significantly relative to R3. For example, at $x = -2L_{SZ}$ and $x = -3L_{SZ}$, the alongshore-averaged $\partial T/\partial z$ is reduced 54% and 24%, respectively, relative to the initial stratification, much larger than the 25% and 15% stratification reductions of R3.

The R4 temperature evolution with patchy, near-surface cooling (Figs. 3b2–4b4) and weakening of the stratification (Figs. 3c2–4c4) continues throughout the 48-h simulation as transient rip currents deliver eddies to the inner shelf. By 24 h, significant, near-surface ($z = -1$ m), R4 cooling has reached $x = -5L_{SZ}$ (Fig. 4a2). From 30 to 48 h, a near-surface, cross-shore temperature front has formed near $x = -3L_{SZ}$, separating the onshore largely homogenized waters in the upper 4 m and the still stratified waters farther offshore. At 48 h, the R4 near-surface $T(x, y) \approx 19.2°C$ for $x > -3L_{SZ}$ (Fig. 4b4), significantly cooled ($\Delta T = 0.55°C$) relative to R3 ($\Delta T = 0.30°C$; Fig. 2b2). Offshore of $x = -3L_{SZ}$, the $T = 19°C$ isotherm, originally at $z = -4$ m, is depressed 1–2 m and slopes upward farther offshore (Fig. 4b4). At $x = -2L_{SZ}$, R4 stratification is essentially destroyed (16% of initial stratification), and at $x = -3L_{SZ}$ stratification is similarly reduced (26% of initial stratification). Even farther offshore, the R4 upper 4-m stratification is substantially reduced relative to R3, which is explored further in section 4d.

After examining R4 temperature evolution and variability in the (x, y) and (x, z) planes, the vertical and alongshore structure of the TRC-induced R4 temperature variability is examined in the (y, z) plane at $x = -1.6L_{SZ}$ ($h = 4$ m; Fig. 5). Recall that at 0 h (initial condition) T is alongshore uniform with constant stratification of $\partial T/\partial z = 0.25°C\,m^{-1}$ (Fig. 5a). At 1 h, $T(y, z)$ is patchy with the 19.5°C isotherm raised and lowered ±2 m at the 50–200-m alongshore length scales (Fig. 5a), consistent with patchy $T(x, y)$ (Fig. 3b1). The alongshore temperature variability is largest at depth with alongshore standard deviation of 0.15°C. At $y \approx 700$ m and $y \approx 0$ m, the instantaneous

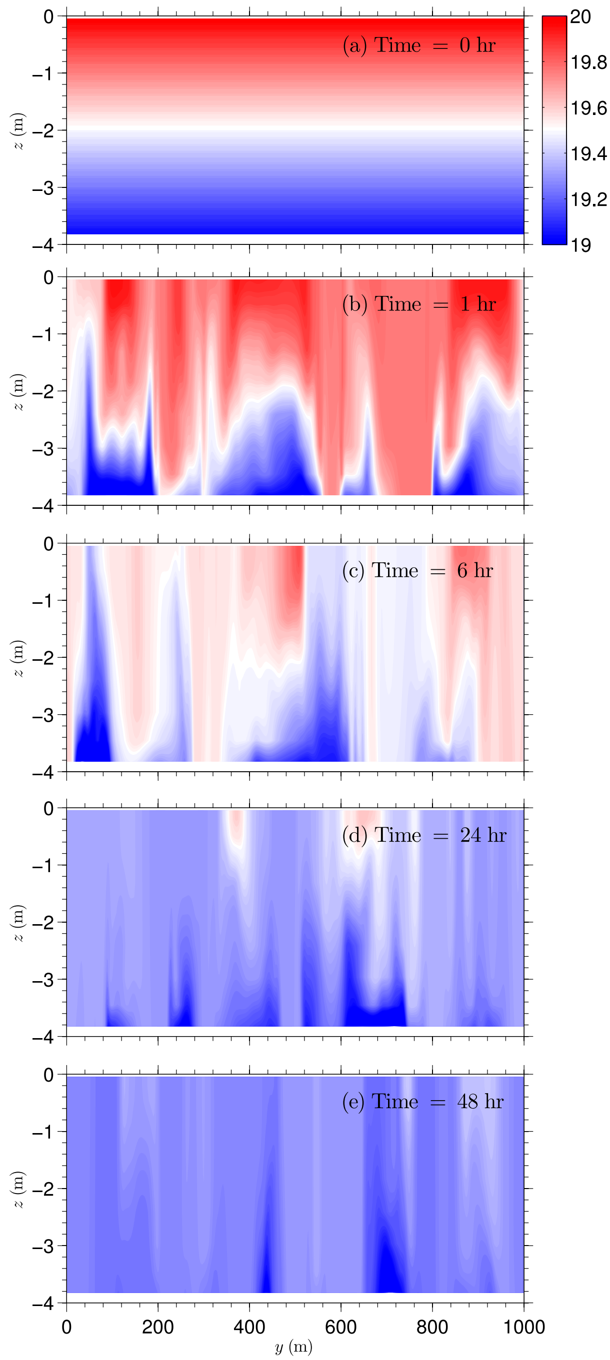

FIG. 5. R4 (with TRCs) simulated temperature at $x = -1.6L_{SZ}$ (−160 m) at (a) 0, (b) 1, (c) 6, (d) 24, and (e) 48 h.

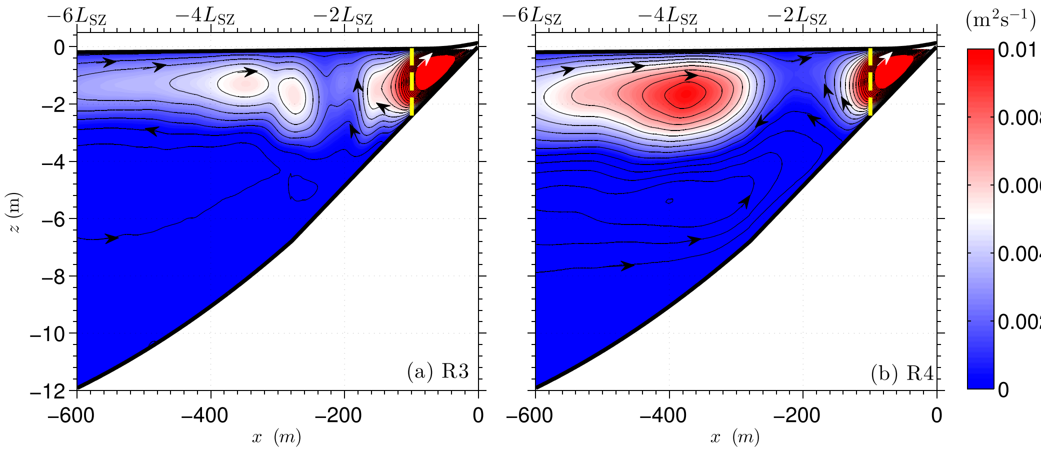

FIG. 6. (a) R3 (no TRCs) and (b) R4 (with TRCs) Lagrangian overturning streamfunction ψ_L (colors and contours at $10^{-3}\,m^2\,s^{-1}$ intervals). Arrows on the contours indicate the direction of the mean Lagrangian velocity, that is, $\overline{u}_L = -\partial\psi_L/\partial z$ and $\overline{w}_L = \partial\psi_L/\partial x$. The averaging is over 12–48 h and the alongshore direction. Dashed vertical yellow line delimits the surfzone $x = -L_{SZ}$.

water column is essentially unstratified. Net cooling is not yet obvious.

At 6 h, R4 $T(y, z)$ has cooled significantly to an (vertical and alongshore) average of 19.35°C, is alongshore patchy with 50–100-m length scales, and is largely unstratified (isotherms are vertical; Fig. 5c). This temperature structure is consistent with observations over $-3 < z < -1$ m 80 m offshore of the surfzone with similar H_s (Hally-Rosendahl et al. 2014). This process of net cooling continues but slows down at 24 h with a mean 19.23°C and 48 h with a mean 19.2°C (Figs. 5d,e). Similarly the temperature alongshore standard deviation decreases from 0.1°C at 1 h to 0.05°C at 48 h. The alongshore T standard deviation is 2 times larger near bed ($z < -3$ m) than in the upper ($z > -2$ m) water column, also consistent with field observations (Hally-Rosendahl et al. 2014).

4. Results: Effects of transient rip currents on a stratified inner shelf—Circulation and temperature statistics

In Part I, TRCs were shown to have a strong effect on inner-shelf velocity variability, vertical viscosity, and exchange flow. The R3 and R4 qualitative temperature evolution comparison (section 3) demonstrates that TRCs have a strong effect on the inner-shelf temperature and stratification to $x = -3L_{SZ}$. Here, the effects of TRCs on the inner-shelf circulation and temperature statistics are quantified with statistics that are alongshore averaged and time averaged from 12 to 48 h (or 12 to 24 h, section 4b). Unlike the unstratified cases in Part I, where equilibrium had been reached and statistics were stationary, here the stratification evolves over the averaging period and thus the statistics are not strictly stationary.

a. Lagrangian mean circulation

As in Part I, a Lagrangian streamfunction ψ_L, defined so that $\overline{u}_L = -\partial\psi_L/\partial z$ and $\overline{w}_L = \partial\psi_L/\partial x$, where $\overline{u}_L$ is averaged over 12–48 h and the alongshore, is used to characterize the effects of Stokes drift and TRCs on the stratified inner-shelf mean Lagrangian circulation (Fig. 6). The inner-shelf stratification has a strong effect on the ψ_L Lagrangian circulation both without (R3) and with (R4) TRCs, relative to an unstratified inner shelf (Part I). Within and just seaward of the surfzone ($>-1.8L_{SZ}$), the R3 $\psi_L(x, z)$ streamlines are closed (Fig. 6a), indicating an overturning circulation pattern with near-surface onshore flow and near-bed offshore flow, consistent with the unstratified case R1 (Part I). Only a few streamlines cross $x = -2L_{SZ}$, and the lower water column ψ_L streamlines are directed upward into the midwater column (Fig. 6a) in contrast to the along-bed offshore flow of the R1 (see Part I). This ψ_L pattern indicates that, without TRCs, stratification acts to an exchange barrier between the surfzone and the inner shelf. Farther offshore $x < -2.5L_{SZ}$, a clockwise ψ_L circulation cell is onshore-directed near the surface and offshore-directed in the midwater column that is largely disconnected from the surfzone (Fig. 6a). Below this upper ψ_L cell, a second weaker counterclockwise ψ_L cell is present with onshore flow near bed. This contrasts with the unstratified no TRC (R1) single inner-shelf ψ_L circulation cell (Part I).

Near the surfzone $x > -1.5L_{SZ}$, R4 (with TRCs) ψ_L is similar to R3 (Fig. 6b). As with R3, few streamlines cross $x = -2L_{SZ}$, also indicating an exchange barrier to the

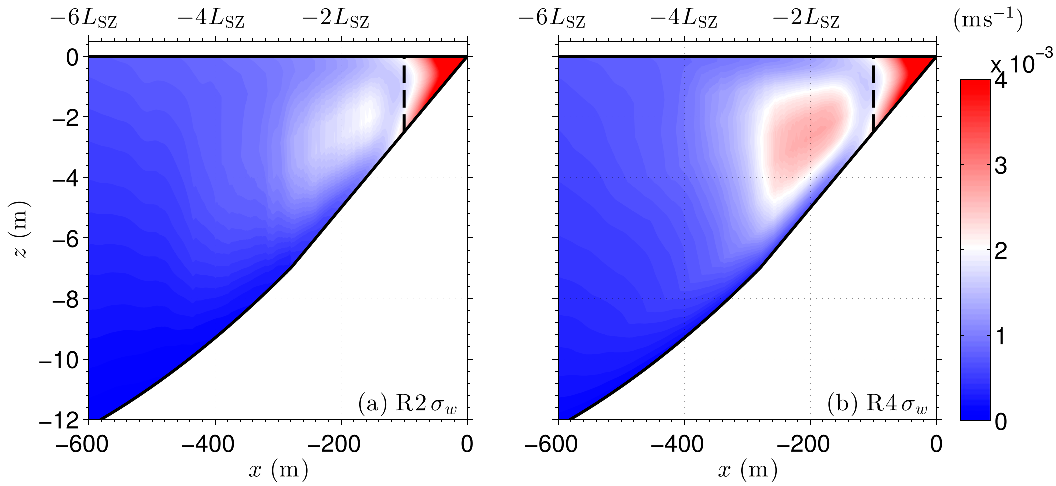

FIG. 7. (a) R2 (no stratification) and (b) R4 (with stratification) simulated vertical Eulerian velocity standard deviation σ_w. The averaging is over 12–24 h and the alongshore direction. Dashed black line delimits the surfzone $x = -L_{SZ}$.

mean $\overline{u}_L$. However, the offshore ($x < -2.5L_{SZ}$) upper clockwise circulation cell is almost twice as strong for R4 as for R3 and extends deeper into the water column (Fig. 6b). The lower counterclockwise circulation is qualitatively similar to R3. This two circulation cell system also contrasts with the unstratified with TRC (R2) ψ_L circulation cell (Part I). The implications of R3 and R4 ψ_L on momentum balances and their relation to observations of Lentz et al. (2008) are discussed in section 5a.

b. Velocity variability

In Part I, the effect of surfzone-generated TRCs on the unstratified inner-shelf velocity variability is quantified with Eulerian cross-shore and vertical velocity standard deviation [$\sigma_u(x, z)$ and $\sigma_w(x, z)$] in simulation R2. Similar to simulation R1 (Part I), R3 is essentially steady. Here, unstratified R2 and stratified R4 $\sigma_u(x, z)$ and $\sigma_w(x, z)$ (averaged over the alongshore and 12–24 h, the duration of R2) are compared to determine the effect of stratification on inner-shelf eddy velocity variability. The R2 $\sigma_u(x, z)$ is described in Part I, and the R4 $\sigma_u(x, z)$ is similar to R2 but slightly reduced (not shown) and is not described further.

In the surfzone ($x = -L_{SZ}$), R2 and R4 $\sigma_w(x, z)$ are similar. In contrast, the unstratified R2 and stratified R4 $\sigma_w(x, z)$ are quite different on the inner shelf at $-4L_{SZ} < x < -L_{SZ}$ (Fig. 7). In this region, R2 σ_w varies from (0.5–2) $\times 10^{-3}$ m s^{-1} (Fig. 7a), with vertical velocities associated with cyclostrophically balanced horizontal eddies (e.g., Burgers 1948; Rott 1958; Sullivan 1959). However, in this region the R4 σ_w is 2 to 3 times stronger than R2, also at maximum in the midwater column (Fig. 7b). Relative to R2, the R4 elevated σ_w is in part due to hydrostatic (i.e., shallow water) internal gravity wave motions that are generated through adjustment to the cyclostrophic eddy-induced raising and lowering of isotherms (e.g., Figs. 3c1, 5b).

c. Vertical eddy viscosity

Stratification inhibits vertical mixing (e.g., Lentz 2001). The ROMS vertical eddy diffusivity K_T and eddy viscosity K_v represent turbulence effects on vertical temperature and momentum mixing. In R3 and R4, the turbulent Prandtl number K_v/K_T is near one and approximately constant. Thus, here the mean eddy viscosity $\overline{K}_v$ (12–48-h time average and alongshore average) is used to examine the role of TRCs in vertical mixing on the stratified inner shelf (Fig. 8).

As in R1 and R2 (Part I), surfzone turbulence in R3 and R4 is principally generated by depth-limited wave breaking. In both R3 and R4, the surfzone ($x > -L_{SZ}$) $\overline{K}_v$ is maximum at $\approx 2 \times 10^{-2}$ m^2 s^{-1} (Fig. 8). Near $x \approx -2L_{SZ}$, the R3 $\overline{K}_v$ is near-surface ($z < -1$ m) intensified at 10^{-3} m^2 s^{-1} and much weaker $O(10^{-5})$ m^2 s^{-1} in the lower water column (Fig. 8). This region separates the two R3 Lagrangian overturning circulation cells (Fig. 6a). Farther offshore near $x \approx -3L_{SZ}$, R3 $\overline{K}_v$ is elevated near 10^{-3} m^2 s^{-1}, extending from the surface to the midwater column ($z = -3$ m), and is much weaker $O(10^{-5})$ m^2 s^{-1} below (Fig. 6a). This enhanced $\overline{K}_v$ corresponds to the downward-directed component of the offshore circulation cell (Fig. 6a).

In contrast, the R4 $\overline{K}_v$ is quasi depth uniform and decays slowly out to $x \approx -3L_{SZ}$ (Fig. 8b). At $x = -2L_{SZ}$, below the surface layer, $z < -1$ m; R4 $\overline{K}_v$ is 100 times

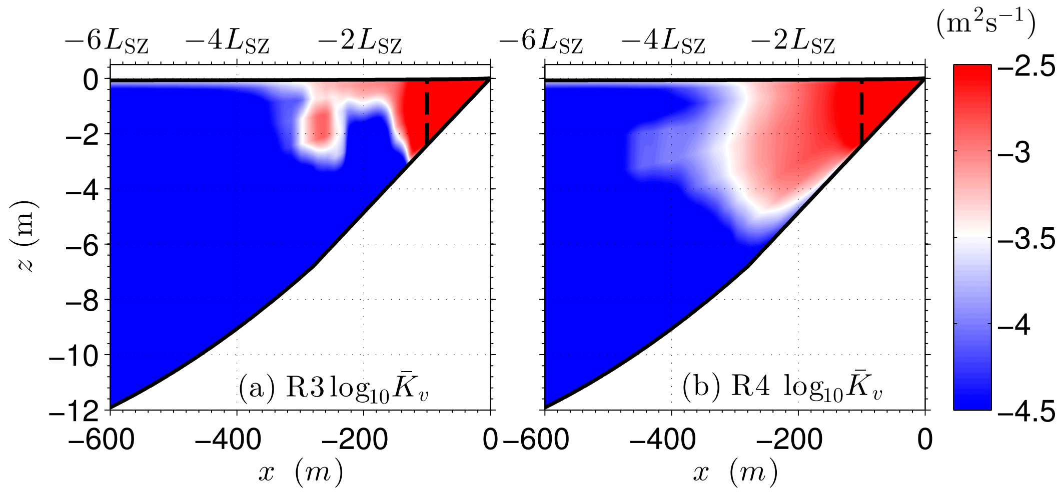

FIG. 8. (a) R3 (no TRCs) and (b) R4 (with TRCs) simulated mean vertical eddy viscosity $\overline{K}_v$ (colored). The averaging is over 12–48 h and the alongshore direction. Dashed black line delimits the surfzone $x = -L_{SZ}$.

stronger than R3 (Fig. 8b). Farther offshore at $x < -4L_{SZ}$, R4 and R3 $\overline{K}_v$ are similar over most of the water column (Fig. 8). However at $x = -4L_{SZ}$ at $z \approx -2.5$ m, R4 $\overline{K}_v$ is weakly elevated due to the Eulerian velocity shear associated with the offshore overturning circulation cell (Fig. 6b). Relative to the unstratified R2 (Part I), the R4 $\overline{K}_v$ is weaker and decays offshore more rapidly, particularly at $x < -3L_{SZ}$.

The R4 elevated $\overline{K}_v$, relative to R3, is in part due to density overturns induced by the inner-shelf eddies ejected by TRCs. R4 eddy vertical velocities raise cold water and spread it laterally (Figs. 3, 4) causing density (temperature) overturns and strongly elevating $\overline{K}_v$ (e.g., Burchard and Bolding 2001). For example, at $x = -2L_{SZ}$, temperature overturns of $\partial T/\partial z < 10^{-3}$°C m^{-1} occurred over the water column 5% of the time for R4 and 0% of the time for R3. This leads to a R4 instantaneous K_v upper range of 10^{-1} m^2 s^{-2} that rapidly mixes the overturn analogous to mixed layer deepening by convective mixing (Burchard and Bolding 2001). At $x = -3L_{SZ}$, R3 has 4% overturning only at $z = -2$ m (and essentially 0% elsewhere in z), which is associated with the downward component of the Lagrangian circulation (Fig. 6a) cell, explaining the elevated $\overline{K}_v$ branch (Fig. 8a). At $x = -3L_{SZ}$, R4 has 2%–4% overturning throughout the water column, also explaining the elevated $\overline{K}_v$ over most of depth (Fig. 8). Overall, TRCs can significantly impact stratified inner-shelf vertical mixing out to $x = -3L_{SZ}$, which likely has implications for tracer exchange across the inner shelf.

d. Mean temperature evolution

Temperature $T(x, z)$ snapshots of R3 (without TRCs, Fig. 2) and R4 (with TRCs, Figs. 3–5) highlight the influence of Lagrangian overturning circulation and TRCs on the evolving temperature field. Here, the (alongshore and 0.5-h time averaged) mean temperature $\overline{T}(x, z)$ for R3 and R4 is examined at 24 and 48 h (Fig. 9) to quantify $\overline{T}$ changes induced by the TRCs. At 24 h, the R3 $\overline{T} = 18$°C and $\overline{T} = 18.5$°C isotherms at deeper depths ($z < -6$ m, Fig. 9a) are largely unchanged from their initial location (Fig. 1a), except near where they contact the seabed. The R3 $\overline{T} = 19$°C isotherm is largely horizontal and is quasi-uniformly depressed downward 0.4 m (Fig. 9a). However, between $-6L_{SZ} < x < -3L_{SZ}$, the $\overline{T} = 19.5$°C isotherm is tilted upward, strongly raising 1.5 m over 300 m cross shore, eventually outcropping between $-3L_{SZ} < x < -2L_{SZ}$ (Fig. 9a). Farther onshore ($x > -2L_{SZ}$), the $\overline{T} = 19.5$°C isotherm falls 3 m over 80 m.

At 24 h, the R4 lower water column $\overline{T} = 18$°C and $\overline{T} = 18.5$°C isotherms are largely similar to R3 (Fig. 9b). In contrast to R3, the R4 $\overline{T} = 19$°C isotherm is depressed between 0.4 and 1.2 m, sloping downward (from offshore to onshore) with a $\Delta z = 0.8$ m over $\Delta x = 250$ m. The R4 $\overline{T} = 19.5$°C isotherm is raised significantly from its original location (at $z = -2$ m) and slopes upward onshore from $z = -1.2$ m at $x = -6L_{SZ}$ to $z = 0$ m at $x = -3.2L_{SZ}$. At $x > -3L_{SZ}$, the R4 water column is significantly more well mixed than for R3 (Figs. 9a,b).

At 48 h, the R3 and R4 temperature evolution continues although less rapidly than in the first 24 h (Figs. 9c,d). The R3 $\overline{T} = 18$°C, $\overline{T} = 18.5$°C, and $\overline{T} = 19$°C isotherms at 48 h is similar at 24 h (Figs. 9a,c). Farther up in the water column, the R3 $\overline{T} = 19.5$°C isotherm has continued to raise and outcrop 50 m farther offshore than at 24 h due to the stirring of the Lagrangian circulation cell's upper branch (Fig. 6a). In contrast, the R4

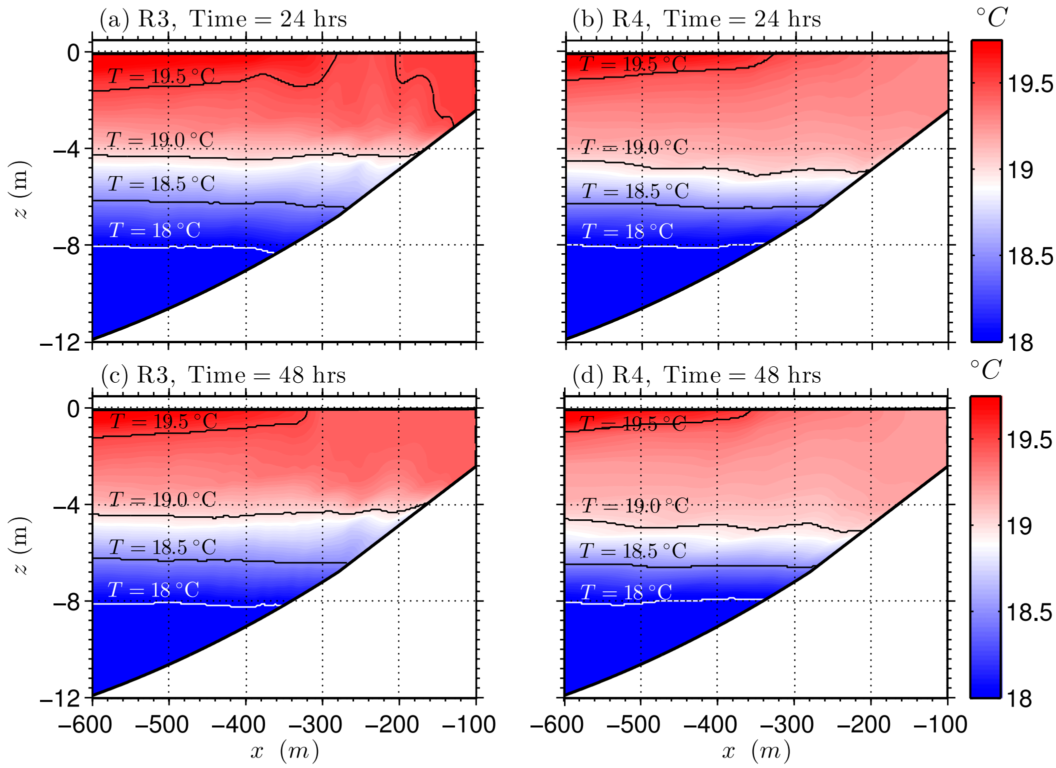

FIG. 9. R3 (no TRCs) and R4 (with TRCs) alongshore-averaged temperature $\overline{T}(x, z)$ at time t = (a),(b) 24 and (c),(d) 48 h. Solid black and white lines (labeled) are temperature contours.

isotherms have evolved significantly at 48 h (cf. Figs. 9b,d). At 48 h, the R4 $\overline{T} = 18.5°\mathrm{C}$ isotherm slopes downward from $z = -6.4$ m at $x = -6L_{\mathrm{SZ}}$ to $z \approx -6.8$ m at $x = -3.5L_{\mathrm{SZ}}$ (Fig. 9d) where no isotherm slope was evident at 24 h (Fig. 9b). At 48 h, the R4 $\overline{T} = 19°\mathrm{C}$ isotherm is on average deeper and is slightly more sloped than at 24 h (Figs. 9b,d). The 48-h R4 $\overline{T} = 19.5°\mathrm{C}$ isotherm was raised higher and outcrops farther offshore than at 24 h. At $x > -6L_{\mathrm{SZ}}$, almost all of the water initially at >19.5°C, with large volume contribution, has been transformed via TRC-driven mixing to lower temperature. Above the $\overline{T} = 19°\mathrm{C}$ isotherm at 48 h, the R4 stratification is strongly reduced relative to R3 at $x > -6L_{\mathrm{SZ}}$.

5. Discussion

Both Stokes drift only (R3) and Stokes drift and TRCs (R4) modify the inner-shelf temperature. However, TRCs (R4) induce substantially larger inner-shelf mean temperature changes out to $x = -6L_{\mathrm{SZ}}$ because of differences in the mean Lagrangian circulation (Fig. 6), the presence of eddies (Fig. 7), and enhanced vertical mixing at $x > -3L_{\mathrm{SZ}}$ (Fig. 8). Even though the R4 eddies and elevated mixing is mostly confined to $x > -3L_{\mathrm{SZ}}$, the strong Lagrangian circulation cell continually brings in offshore water to be transformed and exported, explaining the temperature evolution farther offshore. The implications of Stokes drift and TRCs on stratified inner-shelf momentum balances, mixing, exchange velocity, and along-shelf flow are explored next.

a. Mean momentum balances

As in the unstratified cases in Part I, the effect of Stokes drift and TRCs on the stratified R3 and R4 mean cross-shore and alongshore momentum dynamics is examined at two locations $x = -6L_{\mathrm{SZ}}$ and $x = -3L_{\mathrm{SZ}}$. At $x = -6L_{\mathrm{SZ}}$ ($h = 12$ m), TRCs effects (R4) on mean Lagrangian circulation ψ_L, eddy velocity σ_w, and mean vertical eddy viscosity $\overline{K}_v$ are weak (Figs. 6–8), whereas at $x = -3L_{\mathrm{SZ}}$ ($h = 7.4$ m), TRCs strongly influence σ_u, σ_w, $\overline{K}_v$, and ψ_L. Mean (represented by $\langle\cdot\rangle$) momentum dynamics terms are estimated by an alongshore average and 42–48-h simulation time average. Mean, cross-shore, momentum balance terms examined include mean pressure gradient (PG), Coriolis term, combined advective terms, and vertical mixing (VM). The combined horizontal and vertical advective (ADV) terms are

$$\mathrm{ADV} = -\frac{\partial\langle u_e^2\rangle}{\partial x} - \frac{\partial\langle u_e w_e\rangle}{\partial z}, \qquad (3)$$

where u_e and w_e are Eulerian velocities consisting of mean and eddy contributions $u_e = \overline{u}_e + u'_e$ and $w_e = \overline{w}_e + w'_e$. The mean VM is defined as

$$\mathrm{VM} = \frac{\partial}{\partial z}\left\langle K_v \frac{\partial u_e}{\partial z}\right\rangle. \tag{4}$$

The Coriolis term is $f\overline{v}_e(z)$, where $\overline{v}_e(z)$ is the mean, Eulerian, alongshore current.

At $x = -6L_{\mathrm{SZ}}$ ($h = 12$ m), both R3 and R4 are in a geostrophic balance over depth, that is, the cross-shore PG and the Coriolis term largely balance through the water column (not shown) with magnitude $\approx 10^{-6}\,\mathrm{m\,s^{-2}}$, 4 times stronger than the next largest term. The PG is dominated by a baroclinic component due to the tilting isotherms (Fig. 9), and the associated geostrophic balance is discussed further in section 5d. In contrast to the unstratified R1 and R2 (see Part I), at $x = -6L_{\mathrm{SZ}}$ R3 and R4 are not in a Stokes–Coriolis balance [(1)], due to the enhanced Lagrangian circulation (Fig. 6) forced by the nongeostrophic residual PG.

For the stratified simulations R3 and R4, the cross-shore momentum balance at $x = -3L_{\mathrm{SZ}}$ is different than at $x = -6L_{\mathrm{SZ}}$. It is also different from the unstratified R1 and R2 at $x = -3L_{\mathrm{SZ}}$ (Part I). For R3 (no TRCs), the cross-shore PG approximately balances ADV throughout the water column (solid black and red, Fig. 10) with magnitude $\approx 2 \times 10^{-6}\,\mathrm{m\,s^{-2}}$. The PG has a significant baroclinic component and changes sign at $z = -2.2$ m (Fig. 10). At $z > -2$ m, the negative PG decelerates the onshore current leading to the closed ψ_L circulation cell (Fig. 6). The vertical mixing term VM is weak (not shown) as stratification reduces the vertical eddy viscosity (Fig. 8a), and the Coriolis term is weak.

At $x = -3L_{\mathrm{SZ}}$, the R4 (with TRCs) momentum balance has cross-shore PG, which balances ADV throughout the water column (dashed red and black, Fig. 10) but with a relatively more barotropic vertical structure that does not change sign. This is because TRCs, as in R2, induce a barotropic PG. The R4 vertical advective term $\partial\langle u_e w_e\rangle/\partial z$ is about half that of $\partial\langle u_e^2\rangle/\partial x$. In contrast to the unstratified R2 where VM [(4)] was as large as ADV, the stratified R4 VM term is one-quarter of the ADV term, due to the reduced $\overline{K}_v$ (Part I). Between $-6L_{\mathrm{SZ}} < x < -3L_{\mathrm{SZ}}$, the R3 and R4 mean cross-shore momentum dynamics changes from advection dominated to geostrophy dominated regime. At $x = -3L_{\mathrm{SZ}}$, a Stokes–Coriolis balance does not occur in either R3 or R4.

For the stratified R3 and R4, the lack of a Stokes–Coriolis balance [(1)] either at $x = -3L_{\mathrm{SZ}}$ or $x = -6L_{\mathrm{SZ}}$ contrasts with the Stokes–Coriolis balance at both locations for the unstratified R1 (without TRCs) and at $x = -6L_{\mathrm{SZ}}$ for the unstratified R2 (with TRCs). This result is consistent with h = 12-m depth observations for weak winds where Stokes–Coriolis balance [(1)] with $\overline{u}_e = -\overline{u}_{\mathrm{st}}$ held for unstratified (winter) but did not hold for stratified (summer) conditions (Lentz et al. 2008). The lack of Stokes–Coriolis balance in stratified conditions was unexpected as stratification reduces vertical mixing and should allow for a Stokes–Coriolis balance to dominate. For stratified conditions, observed onshore $\overline{u}_e$ was enhanced (onshore $\overline{u}_L$) at $z < -5$ m and offshore $\overline{u}_e$ was enhanced (offshore $\overline{u}_L$) at $-4 < z < -2$ m, relative to a Stokes–Coriolis balance (Lentz et al. 2008). The observed $\overline{u}_L$ pattern is consistent with the R3 and R4 mean Lagrangian circulation pattern around $x = -6L_{\mathrm{SZ}}$ (Fig. 6). This suggests that the observed summertime inner-shelf deviations from a Stokes–Coriolis balance is due to cross-shore baroclinic pressure gradients induced by surfzone processes.

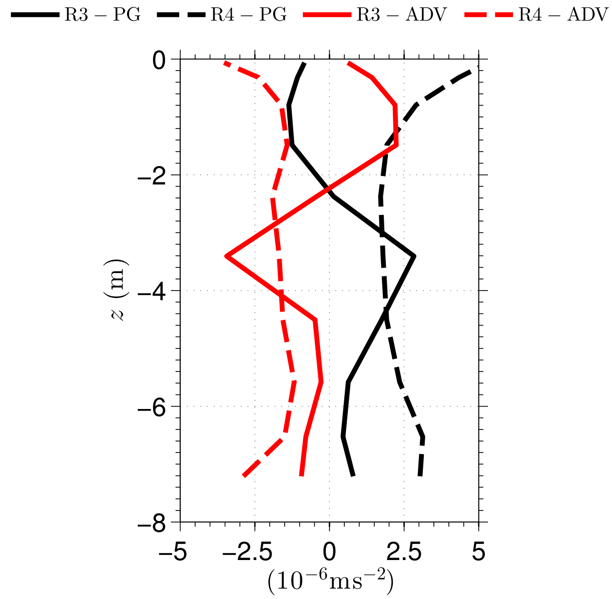

FIG. 10. R3 (solid, no TRCs) and R4 (dashed, with TRCs) mean cross-shore momentum balance terms (PG and ADV) at $x = -3L_{\mathrm{SZ}}$. PG (black) represents the cross-shore pressure gradient. ADV (red) is the sum of horizontal and vertical momentum advection $-\partial\langle u_e^2\rangle/\partial x - \partial\langle u_e w_e\rangle/\partial z$ that includes both Eulerian mean and eddy contributions ($u_e = \overline{u}_e + u'_e$ and $w_e = \overline{w}_e + w'_e$). The averaging is over 42–48 h and the alongshore direction.

b. *Potential energy and irreversible mixing*

In both R3 and R4, the inner-shelf stratification weakens and for $x > -3L_{\mathrm{SZ}}$ temperature cools (Fig. 9), indicating potentially both irreversible mixing and offshore heat (or buoyancy) export. Water column buoyancy can be quantified with a depth-integrated, time- and cross shore–dependent potential energy $e_p(x, t)$:

$$e_p(x,t)=\int_{-h}^{\overline{\eta}}[\overline{\rho}(x,z,t)-\rho_0]g(z+h)\,dz, \qquad (5)$$

where $\overline{\rho}$ is the alongshore-averaged density derived from temperature, $\rho_0 = 1024.5\,\mathrm{kg\,m^{-3}}$, and $\overline{\eta}$ is the mean sea surface elevation. The change in water column potential energy $\Delta e_p(x, t) = e_p(x, t) - e_p(x, t = 0)$ occurs due to both diabatic (irreversible) mixing and cross-shelf buoyancy fluxes induced by Stokes drift and TRCs. Here, R3 and R4 $\Delta e_p(x)$ at times 24 and 48 h are considered (Fig. 11) from the edge of the surfzone ($x = -L_{\mathrm{SZ}}$) to $x = -6L_{\mathrm{SZ}}$.

After 24 h, the R3 Δe_p is $\approx 3.3\,\mathrm{J\,m^{-2}}$ at $x = -L_{\mathrm{SZ}}$ with maximum $\approx 6\,\mathrm{J\,m^{-2}}$ at $-3L_{\mathrm{SZ}} < x < -2.2L_{\mathrm{SZ}}$ (solid black, Fig. 11). The Δe_p increases partly because of the increased water depth. Farther offshore the 24 h R3 Δe_p decreases to $\approx 3\,\mathrm{J\,m^{-2}}$ at $x = -6L_{\mathrm{SZ}}$, even though water depth continues to increase. The R3 positive Δe_p is consistent with the R3 stratification reduction that is strongest for $x > -3L_{\mathrm{SZ}}$ (Fig. 9a). After 48 h, R3 Δe_p (black dashed in Fig. 11) is about 1.5 times the 24-h R3 Δe_p, indicating that the rate of potential energy increase has slowed relative to the first 24 h. The 48-h R3 maximum $\Delta e_p \approx 9\,\mathrm{J\,m^{-2}}$ is near $x = -3L_{\mathrm{SZ}}$ (Fig. 11), where the Lagrangian circulation is downward (Fig. 6a) and mean eddy diffusivity $\overline{K}_v$ is enhanced (Fig. 8a), reducing the stratification.

In contrast, the R4 Δe_p is substantially enhanced at all cross-shore locations relative to R3 at both 24 and 48 h. After 24 h, the R4 Δe_p is 1.5 to 2 times larger than R3 between $-3L_{\mathrm{SZ}} < x < -L_{\mathrm{SZ}}$ (solid red line, Fig. 11), where TRCs have the most impact on vertical velocity variability (Fig. 7b) and $\overline{K}_v$ (Fig. 8b). This region ($x > -3L_{\mathrm{SZ}}$) corresponds to a direct TRC influence region. Farther offshore, the R4 Δe_p also decays and at $x = -6L_{\mathrm{SZ}}$ is similar to the R3 Δe_p, indicating that TRC indirect influence is not yet strong this far offshore (i.e., $x < -3L_{\mathrm{SZ}}$).

After 48 h, the R4 Δe_p is only moderately larger than at 24 h for $x > -1.5L_{\mathrm{SZ}}$, indicating that the processes responsible for stirring in this region are on shorter time scales and thus mostly saturate within 24 h. However, the 48-h R4 Δe_p is substantially larger (1.3 to 1.5 times) at $x < -3L_{\mathrm{SZ}}$ (cf. red solid and dashed, Fig. 11), indicating a stratification weakening process occurring on longer time scales. The 48-h R4 Δe_p is also substantially larger than the 48-h R3 Δe_p (cf. red and black dashed, Fig. 11), particularly from offshore of direct TRC influence $x < -3L_{\mathrm{SZ}}$. Thus, TRCs have strong yet indirect impacts on the inner-shelf temperature (density) field even out to $x = -6L_{\mathrm{SZ}}$. This occurs because of the strong mixing at $x > -3L_{\mathrm{SZ}}$ (Fig. 8b, particularly in the surfzone on shorter time scales), creating cross-shore

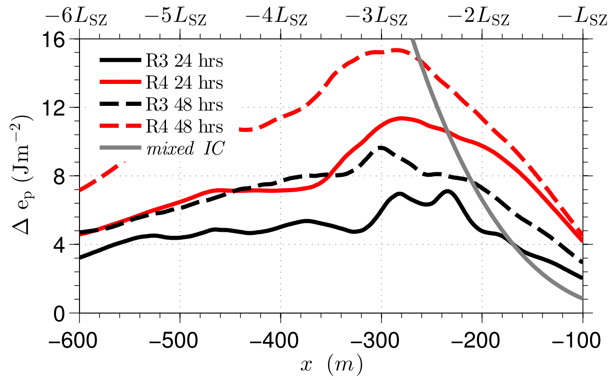

FIG. 11. R3 (black, no TRCs) and R4 (red, with TRCs) alongshore-averaged potential energy change Δe_p after 24 (solid) and 48 h (dashed) of simulation. Gray curve (mixed IC) represents the potential energy increase if the initial temperature profile was fully vertically mixed.

temperature gradients (Fig. 9b), which induce enhanced ψ_L (Fig. 6b) and cross-shelf buoyancy fluxes at longer non-TRC time scales.

For reference, the R3 and R4 increases in potential energy Δe_p are compared to the potential energy increase that would occur if the initial (constant $\partial T/\partial z$) temperature profile (Fig. 1a) were completely vertically mixed at that cross-shore location (denoted as mixed IC, solid gray in Fig. 11). The intersection of this curve with $\Delta e_p(x)$ indicates the cross-shore location where the Δe_p is equivalent to fully mixed initial condition. For R3, this intersection occurs at $x = -1.7L_{\mathrm{SZ}}$ at 24 h and $x = -2.1L_{\mathrm{SZ}}$ at 48 h (Fig. 11). Reflecting the enhanced stirring and mixing effects of TRCs, the R4 intersection occurs farther offshore at $x = -2.3L_{\mathrm{SZ}}$ ($h = 5.75$ m) at 24 h and $x = -2.6L_{\mathrm{SZ}}$ ($h = 6.5$ m) at 48 h (Fig. 11). For both R3 and R4, intersection locations are not unstratified (Fig. 9), demonstrating that heat (buoyancy) is being exported offshore by TRCs and the mean Lagrangian circulation, consistent with field observations (Hally-Rosendahl et al. 2014; Sinnett and Feddersen 2014).

Although R4 Δe_p is larger than R3 at all cross-shore locations, the sloping isotherms (Fig. 9) imply that a part of the potential energy increase is due to adiabatic processes and not irreversible mixing. Here, the role of TRCs and Stokes drift in inducing irreversible mixing is examined via changes in the background potential energy E_b, the minimum potential energy attainable by an adiabatic redistribution of density (Winters et al. 1995). In a closed system, only an irreversible mixing changes the background potential energy. Here, the alongshore normalized E_b (joules per meter) is estimated by sorting the model density and the associated grid volume and calculating (Winters et al. 1995)

$$E_b(t) = \frac{\int (\rho^* - \rho_0) g (z^* + h)\, dV^*}{L_y}, \qquad (6)$$

where ρ^*, dV^*, and z^* are the sorted density, grid cell volume, and vertical coordinate, respectively; $\rho_0 = 1024.5\,\mathrm{kg\,m^{-3}}$; and the integral is over the entire sorted model volume. For R3 and R4, $E_b(t)$ is estimated every five minutes and the initial $E_b(t = 0)$ is subtracted to give $\Delta E_b(t)$ (Fig. 12). Similarly, the total potential energy ΔE_p is the cross shore–integrated e_p,

$$\Delta E_p(t) = \int \Delta e_p(x, t)\, dx, \qquad (7)$$

over the model domain. The available potential energy ΔE_a reflects adiabatic potential energy increases and is the difference between total and background potential energy (i.e., $\Delta E_a = \Delta E_p - \Delta E_b$).

The R3 ΔE_b increases monotonically to $8125\,\mathrm{J\,m^{-1}}$ at 48 h (solid black in Fig. 12). Prior to 1 h, R3 ΔE_b is near zero as the model spins up and enhanced total Δe_p is mostly all available potential energy. Over the next 19 h, $\Delta E_b(t)$ increases quasi linearly at a rate of $210\,\mathrm{J\,m^{-1}\,h^{-1}}$ as the surfzone ($x \geq -L_{SZ}$) strongly mixes (Fig. 8b) and the Stokes drift–driven Lagrangian circulation cell develops exchanging water with the surfzone. At 24 h, the available potential energy is 4% of the total, indicating that most of the Δe_p increase (Fig. 11) is due to irreversible mixing. Thereafter, from 30 to 48 h, $\Delta E_b(t)$ increases relatively slowly at a rate of $120\,\mathrm{J\,m^{-1}\,h^{-1}}$. This $\Delta E_b(t)$ deceleration occurs because the near surfzone ($x > -1.5L_{SZ}$) with enhanced $\overline{K}_v$ (Fig. 8) is already overmixed (Fig. 11). In addition, cross-shore exchange with offshore is limited as very few Lagrangian streamlines cross $x = -2.3L_{SZ}$ (Fig. 6a). Thus, most of the later R3 irreversible mixing (requiring elevated K_v) occurs near $x = -3L_{SZ}$, where R3 $\overline{K}_v$ is enhanced (Fig. 8). At 48 h, the available potential energy is 1% of the total, indicating nearly all of the Δe_p increase is due to mixing.

The R4 ΔE_b increases to $11\,420\,\mathrm{J\,m^{-1}}$ at 48 h (solid red in Fig. 12), overall much more rapidly than for R3, indicating stronger irreversible mixing. Initially R4 ΔE_b is near zero for 1 h as the model spins up, and almost all Δe_p is adiabatic (reversible mixing). However, from 2 to 8 h, ΔE_b increases rapidly (Fig. 12) at $438\,\mathrm{J\,m^{-1}\,h^{-1}}$, twice that of R3 as TRCs exchange surfzone and inner-shelf water (Hally-Rosendahl et al. 2015; Hally-Rosendahl and Feddersen 2016) and export elevated surfzone turbulence. Thereafter, between 10 and 24 h, a transition occurs and ΔE_b increases more slowly at $290\,\mathrm{J\,m^{-1}\,h^{-1}}$, still 1.5 times more rapidly than R3. This occurs as TRCs overmix out to $x = -2.4L_{SZ}$ (red solid, Fig. 11). At 24 h, the available potential energy is 7% of the total, again indicating most ΔE_p increase is due to mixing.

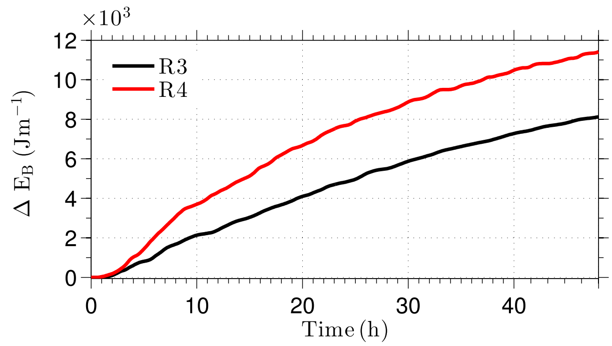

FIG. 12. R3 (black, no TRCs) and R4 (red, with TRCs) alongshore normalized change in background potential energy ΔE_b.

Later, from 30 to 48 h, ΔE_b continues to decelerate at $145\,\mathrm{J\,m^{-1}\,h^{-1}}$ (Fig. 12), only 1.2 times that of R3. The 30–48-h similar R3 and R4 ΔE_b increase masks the spatial differences in increased Δe_p (Fig. 11). For example, from 24 to 28 h, the region $x > -2L_{SZ}$ is still increasing in potential energy in R3 but not in R4 as TRCs have shortened the mixing time scale (Fig. 11). In the region $-6L_{SZ} < x < -3L_{SZ}$, the 24–48-h R4 Δe_p increase is much larger than R3, reflecting the enhanced Lagrangian circulation and mixing both directly and indirectly induced by TRCs. At 48 h, nearly all of the Δe_p increase is due to irreversible mixing, as the available potential energy is 2% of the total.

c. Cross-shelf exchange velocity

On alongshore, uniform bathymetry, both transient rip currents (Hally-Rosendahl et al. 2015; Suanda and Feddersen 2015) and the mean Lagrangian overturning circulation are potential cross-shore exchange mechanisms across the unstratified (Part I) and stratified inner shelves. In Part I, cross-shelf exchange across an unstratified inner shelf was quantified with a cross-shelf exchange velocity U_{ex} (e.g., MacCready 2011; Hally-Rosendahl et al. 2014; Suanda and Feddersen 2015), defined as

$$U_{ex}(x) = \left\langle \frac{-1}{(h + \eta)} \int_{-h}^{\eta} u_L^-(x, y, z, t)\, dz \right\rangle, \qquad (8)$$

where u_L^- is the instantaneous offshore directed u_L (and is zero for onshore u_L), η is the sea surface elevation, and $\langle\cdot\rangle$ represents a time and alongshore average. On the unstratified inner shelf, TRC contributions (simulation R2) to cross-shelf exchange dominated over the mean Lagrangian circulation (simulation R1) out to $6L_{SZ}$. Here, the relative importance of these mechanisms is quantified on the stratified inner shelf, where $U_{\mathrm{ex}}(x)$ is calculated over 12–48 h for R3 and R4.

As in the unstratified inner shelf without TRCs (simulation R1; see Part I), the stratified R3 mean Lagrangian circulation (Fig. 6a) results in a nonzero cross-shore exchange velocity $U_{\mathrm{ex}}^{(\mathrm{R3})}$ (black curves, Fig. 13). For $x > -2L_{\mathrm{SZ}}$, the stratified R3 and unstratified R1 $U_{\mathrm{ex}}(x)$ are similar with surfzone maximum and offshore decay. Near $x = -2L_{\mathrm{SZ}}$, $U_{\mathrm{ex}}^{(\mathrm{R3})}$ is slightly weaker than $U_{\mathrm{ex}}^{(\mathrm{R1})}$, corresponding to the few ψ_L streamlines crossing this region (Fig. 6a). However, farther offshore ($-6L_{\mathrm{SZ}} < x < -2.5L_{\mathrm{SZ}}$), the stratified $U_{\mathrm{ex}}^{(\mathrm{R3})}$ is enhanced 2–3 times over $U_{\mathrm{ex}}^{(\mathrm{R1})}$ as both decay offshore (black solid and dashed curves, Fig. 13), indicating that without TRCs, stratification enhances the Stokes drift–induced cross- and inner-shelf exchange. The mean momentum balance analysis (section 5a) indicates that $U_{\mathrm{ex}}^{(\mathrm{R3})}$ is enhanced because the cross-shore PG prevents a Stokes–Coriolis balance [(1)] from developing.

As with the unstratified inner shelf with TRCs (R2; see Part I), the stratified R4 with TRCs results in an elevated $U_{\mathrm{ex}}(x)$ (Fig. 13) that is at maximum within the surfzone and decays quasi-exponentially offshore. For $x > -4L_{\mathrm{SZ}}$, the stratified $U_{\mathrm{ex}}^{(\mathrm{R4})}$ and unstratified $U_{\mathrm{ex}}^{(\mathrm{R2})}$ are similar (red curves, Fig. 13). However, farther offshore $x < -5L_{\mathrm{SZ}}$; $U_{\mathrm{ex}}^{(\mathrm{R4})}(x)$ is elevated over $U_{\mathrm{ex}}^{(\mathrm{R2})}(x)$ because of the stratification-enhanced mean Lagrangian circulation (Fig. 6b). Analogous to the unstratified R1 and R2, the R4 with TRCs results in $U_{\mathrm{ex}}^{(\mathrm{R4})}$ that is an order of magnitude stronger than $U_{\mathrm{ex}}^{(\mathrm{R3})}$ between $-2.5L_{\mathrm{SZ}} < x < -1.5L_{\mathrm{SZ}}$ (cf. red and black dashed curves, Fig. 13). This demonstrates that, as with unstratified inner shelves (Part I), neglecting TRCs on the stratified inner shelf will result in substantially weaker simulated surfzone to inner-shelf exchange of larvae, sediment, or pollutants. Farther offshore $x < -4L_{\mathrm{SZ}}$, $U_{\mathrm{ex}}^{(\mathrm{R4})}$ is about 2 times larger than $U_{\mathrm{ex}}^{(\mathrm{R3})}$ as the exchange is dominated by the mean Lagrangian circulation set up by the baroclinic cross-shelf pressure gradients (Fig. 10), which are larger with TRCs. Overall, this shows the importance of TRCs of cross-shelf exchange across the inner shelf.

d. *Thermal wind balance*

The R4 mean (alongshore and 42–48-h averaged) alongshore Eulerian velocity $\overline{v}_e(x, z)$ without rotation (i.e., $f = 0$) is expected to be zero as there are no net alongshore forcing mechanisms. However, with rotation, a R4 $\overline{v}_e$ alongshore jet forms (Fig. 14a) between $-7L_{\mathrm{SZ}} < x < -4.5L_{\mathrm{SZ}}$ that is 4 m thick centered at $z = -2$ m with magnitude of 0.03 m s^{-1}, stronger than $\overline{u}_e$. Farther onshore ($x > -4.5L_{\mathrm{SZ}}$), the $|\overline{v}_e| < 0.01$ m s^{-1} is weak and of opposite sign (Fig. 14a). A weaker R3 $\overline{v}_e$ jet also forms (not shown). The alongshore jet results

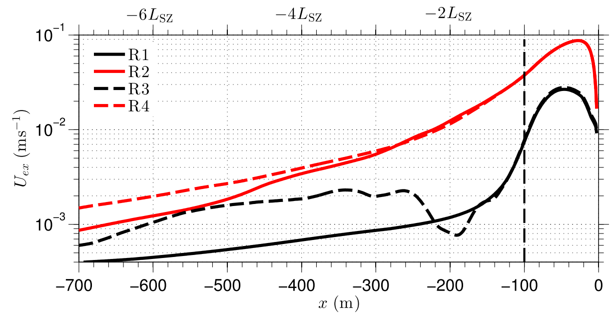

FIG. 13. Exchange velocity U_{ex} [(8) in Part I] for unstratified simulations R1 (black, no TRCs) and R2 (red, with TRCs) and the stratified simulations R3 (dashed black, no TRCs) and R4 (dashed red, with TRCs). Dashed black line delimits the surfzone $x = -L_{\mathrm{SZ}}$.

from the largely geostrophic balance, as discussed in section 5a at $x = -6L_{\mathrm{SZ}}$, as R3 and R4 mean cross-shore temperature gradients $\partial\overline{T}/\partial x$ (Fig. 9) lead to baroclinic pressure gradients that are stronger in R4. If the mean alongshore current is in geostrophic balance, then the thermal wind relationship is expected to hold

$$\frac{\partial \overline{v}_g}{\partial z} = \frac{g\alpha_T}{f}\frac{\partial \overline{T}}{\partial x}, \tag{9}$$

where α_T is the thermal expansion coefficient, and $\overline{v}_g$ is the thermal wind–based geostrophic alongshore current. The thermal wind relationship [(9)] has been observed on the northern California outer shelf (e.g., Winant et al. 1987). On the North Carolina mid- to inner shelf in summer and early fall, the thermal wind balance was found to approximately hold ($r^2 = 0.43$) in the midwater column across 26–8-m water depth (Lentz et al. 1999).

The ability of the thermal wind relationship to predict the $\overline{v}_e$ jet is examined by estimating the R4 thermal wind–based geostrophic alongshore velocity $\overline{v}_g$ by vertically integrating (9), assuming near-bed $\overline{v}_g = 0$ (Fig. 14b) and using the R4 mean (alongshore and 42–48 h averaged) temperature $\overline{T}$. In the region of direct TRC influence ($x > -3L_{\mathrm{SZ}}$), the cross-shore momentum dynamics are complex (Fig. 10b), with time scales much shorter than inertial. Thus, in this region a thermal wind balance (9) is not appropriate, and the thermal wind–derived $\overline{v}_g$ does not resemble $\overline{v}_e$ (Fig. 14). However, farther offshore ($x < -4.5L_{\mathrm{SZ}}$), the thermal wind–derived $\overline{v}_g$ has an alongshore jet with width, vertical location, and magnitude similar although somewhat stronger than the modeled $\overline{v}_e$ (Fig. 14). The modeled $\overline{v}_e$ may be weaker than $\overline{v}_g$ because insufficient time relative to rotational time scales has elapsed.

This agreement between $\overline{v}_g$ and $\overline{v}_e$ indicates that the inner shelf at $x < -4.5L_{\mathrm{SZ}}$ is in a thermal wind balance

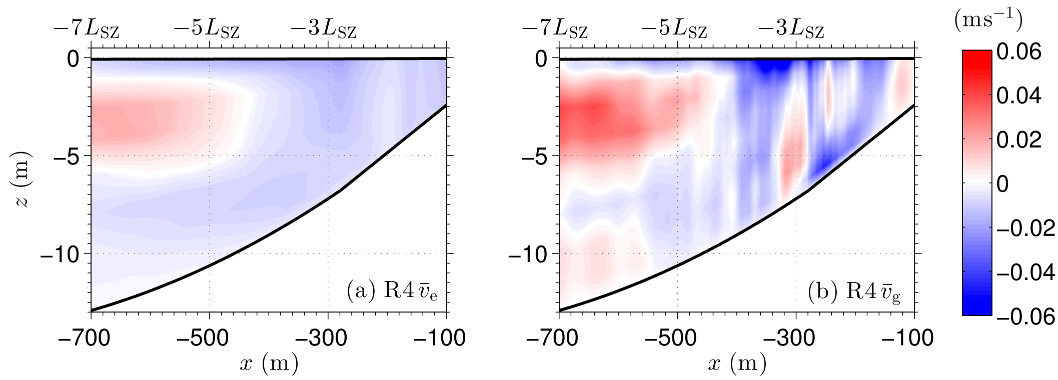

FIG. 14. R4 (a) modeled mean alongshore velocity $\overline{v}(x, z)$ and (b) mean temperature and thermal wind–derived [(9)] geostrophic alongshore velocity $\overline{v}_g$. The mean is defined as an alongshore and 42–48-h average.

whose cross-shore pressure gradients are induced by surfzone processes. Surface wave breaking induces vertical mixing and generates TRCs ejected onto the inner shelf. The presence of a shoreline induces a return Eulerian flow that is not in Stokes–Coriolis balance. This work suggests that surfzone processes must be considered in analysis of stratified inner shelves even in 12-m water depth.

e. Closing thoughts

The inner shelf is a complex region with many forcing mechanisms. These results show the importance of Stokes drift and TRCs on the unstratified and stratified inner shelf. Models for larval, nutrient, or pollution transport that do not include TRC effects will not accurately simulate surfzone to inner-shelf tracer exchange. Furthermore, models that do not include the surfzone and at a minimum Stokes drift, will not accurately simulate even the stratified inner-shelf region at $x = -6L_{SZ}$. These simulations are simplified by neglecting the effects of wind (e.g., Lentz and Fewings 2012), diurnal solar heating and cooling, Langmuir cell circulations (e.g., Gargett and Wells 2007; Tejada-Martínez and Grosch 2007), internal tides and nonlinear internal waves (e.g., Lucas et al. 2011; Wong et al. 2012; Walter et al. 2012; Sinnett and Feddersen 2014; Kumar et al. 2015a; Arthur and Fringer 2016), and rip channel bathymetry (Brown et al. 2015), which can contribute to inner-shelf velocity and temperature variability. Only a single, steady, incident wave field (H_s, $\overline{\theta}$, and σ_θ) is considered. For normally incident waves, varying H_s and σ_θ have a strong impact on TRC-induced exchange on the inner shelf (Suanda and Feddersen 2015). Last, here in Part II, the initial stratification is also not varied. Varying these parameters will strongly affect the circulation, eddies, mixing, and stratification evolution on the inner shelf.

6. Summary

In this two-part study, a depth-integrated, wave-resolving, Boussinesq model funwaveC is coupled to a 3D, wave-averaged ocean circulation and wave propagation model COAWST to diagnose Stokes drift and transient rip current (TRC) effects on an unstratified (Part I) and a stratified (this work, Part II) inner shelf. In Part I, two unstratified simulations were performed without (R1) and with (R2) TRC effects. Here, analogous stratified simulations without (R3) and with (R4) TRC effects are performed; R3 cross-shore temperature evolves slowly due to mean Lagrangian circulation (Stokes drift and offshore-directed undertow). R4 has TRCs that eject onto the inner shelf with eddies out to 4 times the surfzone width L_{SZ}, inducing patchy, near-surface cooling and vertical isotherm displacement. For both R3 and R4, the mean Lagrangian circulation has two clockwise circulation cells: one surfzone centered and one centered farther offshore of the inner shelf that is stronger in R4. Very few R3 and R4 streamlines cross near $x = -2L_{SZ}$, connecting these two cells, indicating a stratified mean circulation barrier to surfzone to inner-shelf exchange, in contrast to the unstratified R1 and R2 simulations. Inner-shelf vertical velocity variability for stratified R4 is 2 to 3 times stronger than unstratified R2 (with TRC). The R4 mean vertical eddy diffusivity is much larger than for R3 largely due to TRC eddy-induced density overturns. The R4 TRC-enhanced stirring and mixing leads to more rapid mean temperature evolution and more strongly sloped isotherms than with the non-TRC R3.

At $x = -6L_{SZ}$, R3 and R4 mean cross-shore momentum balances are geostrophic, driven by cross-shore baroclinic pressure gradient–induced sloping isotherms. This contrasts with the unstratified (R1 and R2) $x = -6L_{SZ}$ Stokes–Coriolis balance, explaining the summertime (stratified) inner-shelf observed deviation from Stokes–Coriolis balance. An alongshore geostrophic jet develops out to $x = -7L_{SZ}$ that is strongest in R4. Farther onshore, the geostrophic balance transitions to (at $x = -3L_{SZ}$) an R3 and R4 balance between the cross-shore pressure gradient and advective terms, with weaker vertical momentum mixing than the unstratified R1 and R2. The R4 increase in potential energy due to both irreversible mixing and cross-shelf buoyancy fluxes is 1.3 to 2 times stronger than R3 across the inner shelf over 48 h. This indicates that TRCs strongly influence inner-shelf cross-shelf heat flux and mixing. TRCs induce an enhanced R4 cross-shore exchange velocity across the entire inner shelf relative to R3 due to both eddy stirring and the enhanced mean Lagrangian circulation. These results demonstrate the direct and indirect effect that TRCs have on the stratified inner shelf and show that accurate inner-shelf simulations should incorporate these wave-driven surfzone processes.

Acknowledgments. Support for N. Kumar and F. Feddersen was provided by Office of Naval Research (ONR) Grant N00014-14-1-0553. Computational support was provided by the COMPAS/ATLAS cluster maintained by Caroline Papadopoulos and Bruce Cornuelle. K. Winters, S. H. Suanda, P. MacCready, and M. S. Spydell provided useful feedback.

REFERENCES

Arthur, R. S., and O. B. Fringer, 2016: Transport by breaking internal gravity waves on slopes. *J. Fluid Mech.*, **789**, 93–126, doi:10.1017/jfm.2015.723.

Brown, J. A., J. H. MacMahan, A. J. H. M. Reniers, and E. B. Thornton, 2015: Field observations of surf zone–inner shelf exchange on a rip-channeled beach. *J. Phys. Oceanogr.*, **45**, 2339–2355, doi:10.1175/JPO-D-14-0118.1.

Burchard, H., and K. Bolding, 2001: Comparative analysis of four second-moment turbulence closure models for the oceanic mixed layer. *J. Phys. Oceanogr.*, **31**, 1943–1968, doi:10.1175/1520-0485(2001)031<1943:CAOFSM>2.0.CO;2.

Burgers, J. M., 1948: A mathematical model illustrating the theory of turbulence. *Adv. Appl. Mech.*, **1**, 171–199, doi:10.1016/S0065-2156(08)70100-5.

Clark, D. B., S. Elgar, and B. Raubenheimer, 2012: Vorticity generation by short-crested wave breaking. *Geophys. Res. Lett.*, **39**, L24604, doi:10.1029/2012GL054034.

Feddersen, F., 2007: Breaking wave induced cross-shore tracer dispersion in the surfzone: Model results and scalings. *J. Geophys. Res.*, **112**, C09012, doi:10.1029/2006JC004006.

——, 2014: The generation of surfzone eddies in a strong alongshore current. *J. Phys. Oceanogr.*, **44**, 600–617, doi:10.1175/JPO-D-13-051.1.

——, D. B. Clark, and R. T. Guza, 2011: Modeling of surfzone tracer plumes: 1. Waves, mean currents, and low-frequency eddies. *J. Geophys. Res.*, **116**, C11027, doi:10.1029/2011JC007210.

Fewings, M., S. J. Lentz, and J. Fredericks, 2008: Observations of cross-shelf flow driven by cross-shelf winds on the inner continental shelf. *J. Phys. Oceanogr.*, **38**, 2358–2378, doi:10.1175/2008JPO3990.1.

Gargett, A. E., and J. R. Wells, 2007: Langmuir turbulence in shallow water. Part 1. Observations. *J. Fluid Mech.*, **576**, 27–61, doi:10.1017/S0022112006004575.

Guza, R. T., and F. Feddersen, 2012: Effect of wave frequency and directional spread on shoreline runup. *Geophys. Res. Lett.*, **39**, L11607, doi:10.1029/2012GL051959.

Hally-Rosendahl, K., and F. Feddersen, 2016: Modeling surfzone to inner-shelf tracer exchange. *J. Geophys. Res. Oceans*, **121**, 4007–4025, doi:10.1002/2015JC011530.

——, ——, and R. T. Guza, 2014: Cross-shore tracer exchange between the surfzone and inner-shelf. *J. Geophys. Res. Oceans*, **119**, 4367–4388, doi:10.1002/2013JC009722.

——, ——, D. B. Clark, and R. Guza, 2015: Surfzone to inner-shelf exchange estimated from dye tracer balances. *J. Geophys. Res. Oceans*, **120**, 6289–6308, doi:10.1002/2015JC010844.

Horwitz, R., and S. J. Lentz, 2014: Inner-shelf response to cross-shelf wind stress: The importance of the cross-shelf density gradient in an idealized numerical model and field observations. *J. Phys. Oceanogr.*, **44**, 86–103, doi:10.1175/JPO-D-13-075.1.

Johnson, D., and C. Pattiaratchi, 2006: Boussinesq modelling of transient rip currents. *Coastal Eng.*, **53**, 419–439, doi:10.1016/j.coastaleng.2005.11.005.

Kumar, N., and F. Feddersen, 2016: The effect of Stokes drift and transient rip currents on the inner shelf. Part I: No stratification. *J. Phys. Oceanogr.*, **47**, 227–241, doi:10.1175/JPO-D-16-0076.1.

——, G. Voulgaris, J. C. Warner, and M. Olabarrieta, 2012: Implementation of the vortex force formalism in the Coupled Ocean–Atmosphere–Wave–Sediment Transport (COAWST) modeling system for inner shelf and surf zone applications. *Ocean Modell.*, **47**, 65–95, doi:10.1016/j.ocemod.2012.01.003.

——, F. Feddersen, S. Suanda, Y. Uchiyama, and J. McWilliams, 2015a: Mid- to inner-shelf coupled ROMS–SWAN model–data comparison of currents and temperature: Diurnal and semi-diurnal variability. *J. Phys. Oceanogr.*, **46**, 841–862, doi:10.1175/JPO-D-15-0103.1.

——, ——, Y. Uchiyama, J. McWilliams, and W. O'Reilly, 2015b: Midshelf to surfzone coupled ROMS–SWAN model data comparison of waves, currents, and temperature: Diagnosis of subtidal forcings and response. *J. Phys. Oceanogr.*, **45**, 1464–1490, doi:10.1175/JPO-D-14-0151.1.

Lentz, S. J., 2001: The influence of stratification on the wind-driven cross-shelf circulation over the North Carolina shelf. *J. Phys. Oceanogr.*, **31**, 2749–2760, doi:10.1175/1520-0485(2001)031<2749:TIOSOT>2.0.CO;2.

——, and M. R. Fewings, 2012: The wind- and wave-driven inner-shelf circulation. *Annu. Rev. Mar. Sci.*, **4**, 317–343, doi:10.1146/annurev-marine-120709-142745.

Lentz, S., R. T. Guza, S. Elgar, F. Feddersen, and T. H. C. Herbers, 1999: Momentum balances on the North Carolina inner shelf. *J. Geophys. Res.*, **104**, 18 205–18 240, doi:10.1029/1999JC900101.

——, M. Fewings, P. Howd, J. Fredericks, and K. Hathaway, 2008: Observations and a model of undertow over the inner continental shelf. *J. Phys. Oceanogr.*, **38**, 2341–2357, doi:10.1175/2008JPO3986.1.

Lucas, A., P. Franks, and C. Dupont, 2011: Horizontal internal-tide fluxes support elevated phytoplankton productivity over the inner continental shelf. *Limnol. Oceanogr. Fluids Environ.*, **1**, 56–74, doi:10.1215/21573698-1258185.

MacCready, P., 2011: Calculating estuarine exchange flow using isohaline coordinates. *J. Phys. Oceanogr.*, **41**, 1116–1124, doi:10.1175/2011JPO4517.1.

Marmorino, G. O., G. B. Smith, and W. D. Miller, 2013: Infrared remote sensing of surf-zone eddies. *IEEE J. Sel. Top. Appl. Earth Obs. Remote Sens.*, **6**, 1710–1718, doi:10.1109/JSTARS.2013.2257695.

Olabarrieta, M., J. C. Warner, and N. Kumar, 2011: Wave-current interaction in Willapa Bay. *J. Geophys. Res.*, **116**, C12014, doi:10.1029/2011JC007387.

Omand, M. M., F. Feddersen, P. J. S. Franks, and R. T. Guza, 2012: Episodic vertical nutrient fluxes and nearshore phytoplankton blooms in Southern California. *Limnol. Oceanogr.*, **57**, 1673–1688, doi:10.4319/lo.2012.57.6.1673.

Peregrine, D. H., 1998: Surf zone currents. *Theor. Comput. Fluid Dyn.*, **10**, 295–309, doi:10.1007/s001620050065.

Rott, N., 1958: On the viscous core of a line vortex. *Z. Angew. Math. Phys. ZAMP*, **9**, 543–553, doi:10.1007/BF02424773.

Sinnett, G., and F. Feddersen, 2014: The surf zone heat budget: The effect of wave heating. *Geophys. Res. Lett.*, **41**, 7217–7226, doi:10.1002/2014GL061398.

Spydell, M. S., and F. Feddersen, 2009: Lagrangian drifter dispersion in the surf zone: Directionally spread, normally incident waves. *J. Phys. Oceanogr.*, **39**, 809–830, doi:10.1175/2008JPO3892.1.

Suanda, S. H., and F. Feddersen, 2015: A self-similar scaling for cross-shelf exchange driven by transient rip currents. *Geophys. Res. Lett.*, **42**, 5427–5434, doi:10.1002/2015GL063944.

Sullivan, R. D., 1959: A two-cell vortex solution of the Navier–Stokes equations. *J. Aerosp. Sci.*, **26**, 767–768, doi:10.2514/8.8303.

Tejada-Martínez, A. E., and C. E. Grosch, 2007: Langmuir turbulence in shallow water. Part 2. Large-eddy simulation. *J. Fluid Mech.*, **576**, 63–108, doi:10.1017/S0022112006004587.

Tilburg, C., 2003: Across-shelf transport on a continental shelf: Do across-shelf winds matter? *J. Phys. Oceanogr.*, **33**, 2675–2688, doi:10.1175/1520-0485(2003)033<2675:ATOACS>2.0.CO;2.

Walter, R. K., C. B. Woodson, R. S. Arthur, O. B. Fringer, and S. G. Monismith, 2012: Nearshore internal bores and turbulent mixing in southern Monterey Bay. *J. Geophys. Res.*, **117**, C07017, doi:10.1029/2012JC008115.

Warner, J. C., B. Armstrong, R. He, and J. B. Zambon, 2010: Development of a Coupled Ocean–Atmosphere–Wave–Sediment Transport (COAWST) modeling system. *Ocean Modell.*, **35**, 230–244, doi:10.1016/j.ocemod.2010.07.010.

Winant, C., R. Beardsley, and R. Davis, 1987: Moored wind, temperature, and current observations made during coastal ocean dynamics experiments 1 and 2 over the northern California continental shelf and upper slope. *J. Geophys. Res.*, **92**, 1569–1604, doi:10.1029/JC092iC02p01569.

Winters, K. B., P. N. Lombard, J. J. Riley, and E. A. D'Asaro, 1995: Available potential energy and mixing in density-stratified fluids. *J. Fluid Mech.*, **289**, 115–128, doi:10.1017/S002211209500125X.

Wong, S. H. C., A. E. Santoro, N. J. Nidzieko, J. L. Hench, and A. B. Boehm, 2012: Coupled physical, chemical, and microbiological measurements suggest a connection between internal waves and surf zone water quality in the Southern California Bight. *Cont. Shelf Res.*, **34**, 64–78, doi:10.1016/j.csr.2011.12.005.

Xu, Z., and A. J. Bowen, 1994: Wave- and wind-driven flow in water of finite depth. *J. Phys. Oceanogr.*, **24**, 1850–1866, doi:10.1175/1520-0485(1994)024<1850:WAWDFI>2.0.CO;2.